

A EUROPEAN JOURNAL

CHEMPHYSICHEM

OF CHEMICAL PHYSICS AND PHYSICAL CHEMISTRY

Accepted Article

Title: Linear and Nonlinear Optical Properties of Tricyanopropylidene-based Merocyanine Dyes: Synergistic Experimental and Theoretical Investigations

Authors: Venkatakrishnan Parthasarathy, Ravindra Pandey, Puspendu Kumar Das, Frederic Castet, and Mireille Blanchard-Desce

This manuscript has been accepted after peer review and appears as an Accepted Article online prior to editing, proofing, and formal publication of the final Version of Record (VoR). This work is currently citable by using the Digital Object Identifier (DOI) given below. The VoR will be published online in Early View as soon as possible and may be different to this Accepted Article as a result of editing. Readers should obtain the VoR from the journal website shown below when it is published to ensure accuracy of information. The authors are responsible for the content of this Accepted Article.

To be cited as: *ChemPhysChem* 10.1002/cphc.201701143

Link to VoR: <http://dx.doi.org/10.1002/cphc.201701143>

WILEY-VCH

www.chemphyschem.org

A Journal of



Linear and Nonlinear Optical Properties of Tricyanopropylidene-based Merocyanine Dyes: Synergistic Experimental and Theoretical Investigations

Venkatakrishnan Parthasarathy,^{a,b} Ravindra Pandey,^{c,d} Puspendu Kumar Das,^{*,c}

Frédéric Castet,^{*,e} Mireille Blanchard-Desce^{*,b,e}

^a Department of Chemistry, Indian Institute of Technology Madras, Chennai – 600 036, India.
pvenkat@iitm.ac.in

^b Chimie et Photonique Moléculaire (CNRS, UMR 6510), Université de Rennes 1, 35042
Rennes, France.

^c Department of Inorganic and Physical Chemistry, Indian Institute of Science, Bangalore,
560012, India.

^d Department of Spectroscopy, Indian Association for the Cultivation of Science, Jadavpur,
Kolkata 700032, India

^e University of Bordeaux, Institut des Sciences Moléculaires (CNRS, UMR 5255), 33405
Talence, France.

pkdas@ipc.iisc.ernet.in

frederic.castet@u-bordeaux.fr

mireille.blanchard-desce@u-bordeaux.fr

Abstract

New merocyanines dyes including tricyanopropylidene-based acceptor units connected to dihexylaminophenyl or dihexylaminothiophenyl donor moieties through polyenic bridges of different lengths have been designed. All derivatives exhibit a strong dipolar character and show a typical intramolecular charge transfer (ICT) transition. NMR experiments combined to

DFT calculations demonstrate that the nature of the donor/acceptor pair, as well as the length of the conjugated linker, strongly impact the electronic structure of the dyes, inducing alteration in the bond length alternation (BLA) and marked shifts in the ICT absorption bands. Hyper-Rayleigh scattering experiments reveal an exponential increase of the second-harmonic generation response when enlarging the polyenic chain length. Strikingly, the largest chromophores that incorporate the strongest donor/acceptor pair exhibit giant first hyperpolarizability in combination to a cyanine-like electronic structure, which apparently contradicts the paradigm of optimal BLA predicted by the two-state model. Although it decreases when increasing the polyenic chain length, all dyes also exhibit high thermal stability, which demonstrates their potential for application in nonlinear optical devices.

I. Introduction

The design of organic chromophores displaying large nonlinear optical (NLO) responses have attracted much attention in the chemistry community, due to their potential use as molecular components in optoelectronic devices,¹ or as nonlinear probes for cellular imaging.² For instance, second harmonic scattering, which produces a scattered wave with frequency twice of that of the incident light, is currently exploited in laser components, optical telecommunications, information and signal processing, data storage,³ as well as in bioimaging.⁴ Although large NLO properties have been demonstrated in octupolar systems,⁵ the design of efficient NLO-phores mostly relies on push-pull molecules that contain an electron-donating group (D) interacting with an electron-withdrawing group (A) through π -conjugation. Among them, push-pull polyenes motivated a lot of studies that allowed establishing structure-property relationships linking the magnitude of the second-order NLO response (*i.e.* the quadratic hyperpolarizability β) to the chemical structure of the molecules, highlighting the key role of the relative strength of the D and A groups as well as of the length

of the polyenic chain.⁶ Simple conceptual guidelines for designing such D- π -A polyenic dyes are provided by the two-state model, in which the normalized ground-state wavefunction can be written as a linear combination of the DA and D^+A^- resonance forms:

$$\psi_g = \sqrt{1-\delta}|DA\rangle + \sqrt{\delta}|D^+A^-\rangle \quad (1)$$

with δ the formal charge transfer between D and A. Within this two-state approximation (TSA), the static first hyperpolarizability tensor is expressed as:

$$\beta_{zzz}^{TSA} = 6\mu_{ge}^2\Delta\mu_{ge}/\Delta E_{ge} = 9f_{ge}\Delta\mu_{ge}/\Delta E_{ge}^2 \quad (2)$$

where ΔE_{ge} is the excitation energy between the ground state (g) and the dipole-allowed excited state (e), μ_{ge} is the transition dipole associated to the excitation, $f_{ge} = \frac{2}{3}\Delta E_{ge}\mu_{ge}^2$ is the oscillator strength, and $\Delta\mu_{ge} = |\vec{\mu}_e - \vec{\mu}_g|$ is the change in dipole moment between the two electronic states. This latter quantity can be simply expressed as $\Delta\mu_{ge} = (1-2\delta)\mu_z$, where μ_z is the dipole moment of the D^+A^- resonance structure. Therefore, $\Delta\mu_{ge}$ cancels out in the so-called *cyanine limit*, where the resonant basis states $|DA\rangle$ and $|D^+A^-\rangle$ have identical weights in the ground state wavefunction ($\delta = 1/2$ in Eq. 1). Highly conjugated cyanine-like chromophores showing negligible bond length alternation (BLA) along the polyenic chain are thus expected to display weak second-order NLO responses. In contrast, chromophores exhibiting optimal BLA (≈ 0.05 Å) are expected to behave as effective NLO scatterers.^{4c} However, with the design of original polyenic push-pull derivatives bearing a phthalimide-substituted tricyanopropylidene terminal segment (series **II'** in Chart 1), we demonstrated recently that this BLA/ β paradigm could apparently be overcome.⁷ The longest derivatives were indeed found to display record hyperpolarizabilities (up to 3900×10^{-30} esu from hyper-Rayleigh scattering (HRS) measurements carried out at 1907 nm) although having vanishing BLA, in contrast to previously reported push-pull compounds displaying large β values.^{4c,8} These strongly dipolar dyes were also demonstrated to exhibit good thermal stabilities

together with narrow absorption spectra (and thus improved transparency). Moreover, they were shown to undergo a base-promoted intramolecular cyclization that further enhances their quadratic NLO response and thermal stability, as compared to their non-cyclized analogs having the same number of conjugated double bonds in the polyenic linker.⁹

In this work, we extend this family of compounds by designing new derivatives that involve either a 4-(dihexylamino)phenyl (D1) or a 2-(dihexylamino)thiophenyl (D2) function as donor unit, and a tricyanopropylidene-based acceptor unit incorporating an amine (A1) or a phthalimide (A2) substituent. The connection of these push and pull moieties through polyenic conjugated chains of variable length gives rise to the four series depicted in Chart 1. The linear and nonlinear optical properties, as well as the thermal stability of the three new series **I**, **I'** and **II**, are described herein in comparison to those of their **II'** analogs, reported previously⁷. Quantum chemical calculations are also conducted in order to provide an in-depth understanding of the experimental measurements.

II. Experimental and computational details

II.1 Synthesis of the poly[n]enic chromophores

The synthesis of the push-pull chromophores is described in Scheme 1. The required aldehydes, viz., 4-dihexylaminobenzaldehyde and 5-bromo-2-thiophenecarboxaldehyde, were obtained starting from the 4-dihexylaminobenzene and 5-bromo-2-thiophenecarboxaldehyde by Vilsmeier-Haack formylation and amination, respectively. The vinylogation of these aldehydes was attempted by two different methods: A) by repetitive Wittig oxypropenylation using tributyl-[1,3]-dioxolan-2-ylmethylphosphonium bromide under NaH/THF conditions at optimum temperature followed by removal of the dioxolane moiety by acid hydrolysis, and B) by Wittig oxypropenylation using phosphonium ionic liquid, which can be obtained from Wittig phosphonium salt as shown in Scheme 1 (see the Supporting Information for details), under neat/melt (100 °C) conditions. As the aldehyde functionality in **3a** or **3b** is strongly

deactivated due to the presence of the *N,N*-dihexylamino unit at the donor site, a highly reactive phosphorane was considered necessary so as to have better reactivity. Hence, a slightly modified Spangler's strategy (method A) using tributyl-[1,3]-dioxolan-2-ylmethylenephosphorane instead of triphenyl-[1,3]-dioxolan-2-ylmethylenephosphorane was optimized for series **3a**[*n*] and was adapted further for series **3b**[*n*]. Indeed, this reaction proceeded in an expeditious and facile fashion to attain better yields with complete conversion without any higher homologs or undesired products. Such a transformation is highly encouraged in multistep synthesis due to the minimum or no loss of the precursor enals; the products obtained must be able to be taken to the next step conveniently without any further purification. The method B that involves phosphonium ionic liquid also resulted in reasonable yields. Each olefin-homologated aldehyde (enals), thus obtained at this stage, was further subjected to Knoevenagel condensation with 3-amino-2-cyano-pent-2-enediamine to provide the desired amines (series **I** and **I'**); the condensation proceeded smoothly without any added base. The resulting extended amines were further condensed with phthalic anhydride in presence of triethylamine to afford the desired phthalimide-anchored extended push-pullchromophores, **II** and **II'** (see Supporting Information for details). The polyenic push-pull chromophores (both amines and imides) thus obtained were strongly colored. The results of the above steps have been consolidated in Table 1. All the above compounds were thoroughly characterized by IR, ¹H and ¹³C NMR spectroscopy and mass spectrometry, as reported in the Supplementary Material.

II.2 Quantum chemical calculations

Molecular structures were optimized using density functional theory (DFT) together with the B3LYP exchange-correlation functional (XCF) and the 6-311G(d) basis set. Although the B3LYP XCF has been shown to underestimate the bond length alternation values in long conjugated oligomers,¹⁰ this level of calculation provides reliable general trends when

comparing analogous systems. To save computational time, the *N,N*-dihexylamino units at the donor site of the compounds were replaced by *N,N*-dimethylamino units in all geometry optimizations. Each structure was characterized as a minimum of the potential energy surface on the basis of its real harmonic vibrational frequencies. Vertical excitation energies and excited state properties were determined using time-dependent density functional theory (TDDFT) with the CAM-B3LYP XCF and the larger 6-311+G(d) basis set. The CAM-B3LYP XCF adds a long-range correction to B3LYP using the Coulomb-attenuating method,¹¹ and includes 19% of HF exchange at short-range and 65% at long-range (with a range separating parameter $\mu = 0.33 \text{ a}_0^{-1}$). This long-range correction is known to improve the description of low-lying charge-transfer excited states¹². Dynamic (frequency-dependent) first hyperpolarizabilities were calculated at the same level of approximation using an incident wavelength of 1907 nm, since it was shown to fairly reproduce the second-order NLO properties of a large variety of organic chromophores,¹³ including the enhancement of the HRS hyperpolarizability upon increasing the polymethine chain length in the **II'** series⁷ and in their cyclized derivatives.⁹ Solvent (chloroform) effects were included both in geometry optimizations and calculations of the optical properties by using the Integral Equation Formalism (IEF) version of the Polarizable Continuum Model (IEF-PCM).¹⁴ All calculations were performed using the Gaussian 09 package.¹⁵

III. Geometry and ground state electronic structure of push-pull dyes

The geometry and ground-state electronic structure of the various chromophores were investigated by combining ¹H NMR experiments and DFT calculations. The ¹H NMR spectra recorded in CDCl₃ revealed an all-*trans* configuration of the protons of the polyenic backbone. The ¹H–¹H coupling constants between vicinal protons of the conjugated chain (³*J*_{HH}) deduced from ¹H–¹H COSY experiments, as well as their average differences (ΔJ_{av}), are reported in Table 2. It is known that protons in *anti* configuration linked through a pure

double carbon bond have a typical coupling constant of 16.5 Hz, while ${}^3J_{\text{HH}} = 10.0$ Hz for protons linked through a pure single C–C bond.¹⁶ The coupling constants reported in Table 2, ranging between these two limit values, are typical of conjugated polyenic systems with strong electron delocalization. The average difference values ΔJ_{av} reveal that the oscillatory behavior of the ${}^3J_{\text{HH}}$ values (see also Figure 1) is more pronounced in compounds **I** and **II** than in compounds **I'** and **II'**, which provides evidence for a smaller bond length alternation along the conjugated chain in chromophores incorporating the strongest donor group D2. As previously reported,⁷ the **II'** series involving both the strongest donor (D2) and acceptor (A2) groups exhibits negligible ΔJ_{av} values, and thus appears to be close to the cyanine limit, *i.e.* with a BLA close to zero. Moreover, one observes that the ΔJ_{av} values increase upon increasing the length of the conjugated backbone in series **I** and **I'**, while they decrease in series **II**. In the case of **II'**, ΔJ_{av} lies close to zero independently on the chain length.

To examine the alteration in coupling constants with respect to the solvent polarity, additional ${}^1\text{H}$ NMR experiments were performed in C_6D_6 (less polar) and $\text{C}_3\text{D}_6\text{O}$ (more polar) for the poly[*n*]enic analogs with $n = 1$ as representative cases (Table 3). For **I** and **I'**, the ΔJ_{av} values display a non-monotonic behavior with respect to solvent polarity. For the **II**[1] chromophore, the ΔJ_{av} values decrease with increasing solvent polarity, evidencing a reduction of BLA. In contrast, the ΔJ_{av} values of **II'** remain close to zero independently on the solvent polarity, which further confirms the closeness of the **II'** series to the cyanine limit, with no alteration in BLA.

The bond length alternations calculated at the B3LYP/6-311G(d) level in chloroform (Table 4) are fully consistent with the NMR measurements. For a conjugated chain containing N carbon atoms, the BLA is calculated as:

$$\text{BLA}_{1\dots N} = 1/(N-2) \sum_{i=1}^{N-2} \left\{ (d_{i+1,i+2} - d_{i,i+1}) \times (-1)^{i+1} \right\} \quad (3)$$

where $d_{i,j}$ is the interatomic distance between carbons i and j . Consistently with ${}^1\text{H}$ NMR

experiments, the series **I** and **II** that involve the weaker donor group D1 exhibit larger BLA than **I'** and **II'**, in which the donor is stronger. For a given length of the polyenic chain, the BLA values evolve following the order $\mathbf{I} > \mathbf{II} > \mathbf{I}' > \mathbf{II}'$, supporting the NMR data. In particular, the **II'** series display much smaller BLA values than the other series, confirming its closeness to the cyanine limit. However, within a series, the computed BLA decreases as the polyenic chain length increases until saturation for the longer chains, which contradicts the experimental results for chromophores **I**[*n*] and **I'**[*n*].

Table 4 also reports the calculated ground state dipole moments, the HOMO and LUMO energies and the resulting energy gap, $E_{\text{GAP}} = E_{\text{LUMO}} - E_{\text{HOMO}}$. As expected, increasing the polyenic chain length shifts up and down the HOMO and LUMO levels, respectively, resulting in a lowering of the electronic gap. The ground-state dipole also progressively increases with chain length. Consistent with the relative strengths of the donor and acceptor units, dipole values follow the $\mathbf{I} < \mathbf{II} < \mathbf{I}' < \mathbf{II}'$ ordering, *i.e.* reverse of the BLA values, and reach values exceeding 30 D for the longest derivative of the **II'** series.

IV. Thermal properties

Thermal stability of a chromophore is one of the key requirements for its practical applications. In order to test the potential of the newly synthesized push-pull systems, the thermal properties of the push-pull polyenic chromophores **I**, **I'**, **II** and **II'** were probed by differential scanning calorimetry (DSC), and the transition temperatures (glass transition temperature T_g , crystallization temperature T_c , melting temperature T_m , onset of decomposition T_{od} , and decomposition exotherm, T_d) derived from the thermograms are presented in Table 5. The DSC thermograms for the secondary analogs ($n = 1$) are reported in Figure 2. All merocyanine dyes exhibit a sharp endothermic melting transition and few of them reveal a glass transition. A perusal of the data from Table 5 indicates that the shortest

poly[n]enes generally possess better thermal stabilities (onset of decomposition) than more elongated polyenes, and that the simplest analogs **I**, **I'** and **II'**[0] display decomposition temperature as high as ca. 270 °C. This suggests that shortening the chain length increases the steric congestion and thus reduces the flexibility (or increases the rigidity) around the polyenic backbone, which has for consequence to enhance the thermal stability. The thiophene-based push-pull poly[n]enes incorporating a phthalimide function (**II'**) possess higher thermal stabilities than their amine counterparts **I'**. As previously observed in various molecular systems and polymers,¹⁷ the phthalimide unit affords rigidity to the molecule, locks the geometry and thereby restricts the molecular motion in the solid state, thus resulting in a better stability. However, phenyl-based polyenes do not follow such a trend. Moreover, it is noteworthy that phenyl-based push-pull systems **I** and **II** show better thermal properties than their thiophene analogs **I'** and **II'**.

V. Linear optical properties

V.1 Absorption properties in chloroform

The UV-vis spectra of the different chromophores were recorded in chloroform (ca. 10^{-5} M). As representative examples, chromophores of the **I'** and **II'** series are shown in Figure 3, while the maximum absorption wavelengths measured for all compounds are gathered in Table 6. Depending on the nature of the donor and acceptor groups and on the length of the polyenic chain, the push-pull chromophores exhibit a wide range of absorption maxima, going from the visible to the near-IR region. Within a given series, a marked bathochromic shift is observed upon increasing the conjugation length. In addition, a considerable broadening of the main absorption band is observed as increasing *n* within the series **I**, **I'** and **II**. Intriguingly, the opposite trend is observed for the series **II'**, in which the full-width at half maximum (FWHM) falls as the length of the conjugated chain increases.

Moreover, upon elongation of the backbone, the absorption maximum tends to saturate in the cases of **I** and **I'**. In the **II** and **II'** series, each vinylogation induces a redshift of the absorption maximum by ca. 100 nm, without any saturation. Most notably, the chromophores **II'**[3] and **II'**[4] reveal a near-IR absorption at 916 and 1033 nm, respectively. Figure 4 illustrates the dramatic variation in the absorption maximum within the series **I** → **I'** → **II** → **II'** for the shortest merocyanine derivatives ($n = 0$).

Although the maximal absorption wavelengths are systematically underestimated, TDDFT calculations conducted at the CAM-B3LYP/6-311+g(d) level fairly reproduce their evolution with respect to the nature of the donor and acceptor units, as well as the relative amplitude of the redshift when increasing the polyenic chain length. Consistent with UV/Vis. measurements, the calculated maximal absorption wavelengths evolve in the order $\mathbf{I}[n] < \mathbf{I}'[n] < \mathbf{II}[n] < \mathbf{II}'[n]$ for the same chain length n . As expected for conjugated dyes, the lowest-energy excited state is dominated by a HOMO to LUMO electronic excitation. Both MOs extend over the whole conjugated backbone of the molecules, the LUMOs being shifted towards the tricyanopropylidene withdrawing unit compared to the HOMOs (the shape of the MOs are provided in the supporting information for all compounds). In the **I'** and **II'** series, the frontier MOs do not spread over the phthalimide substituent, since the latter makes an angle of about 60° with the tricyanopropylidene fragment due to steric hindrance. We note also that, within a same series, the weight of the H→L excitation in the first allowed optical transition slightly decreases with increasing n . For a same chain of length n , the H→L contribution is larger in compounds **I'** and **II'** than in their **I** and **II** analogs. The calculated oscillator strengths are larger in **I-II** than in **I'-II'**, and progressively increase with chain length, as a result of the gradual increase of the transition dipole moment. This trend is not fully observed experimentally, where the oscillator strengths, evaluated as $f_{max} \approx 4.3 \times 10^{-9} \times \epsilon \times FWHM$, decrease for the larger chains.

In addition to the theoretical transition wavelengths and oscillator strengths, Table 6 also reports the dipole moment variation between the ground state and the optically active excited state ($\Delta\mu_{ge}$). From the analysis of the total electron densities of the two electronic states, $\Delta\mu_{ge}$ is further decomposed as $\Delta\mu_{ge} = d^{CT} \times q^{CT}$, where q^{CT} is the photo-induced charge transfer, *i.e.* the global amount of charge transferred upon light excitation, and d^{CT} is the distance over which this charge is transferred.¹⁸ For identical chain lengths n , the $\Delta\mu_{ge}$ values decrease in the order $\mathbf{I}[n] > \mathbf{II}[n] > \mathbf{I}'[n] > \mathbf{II}'[n]$, except for $n = 0$ for which the $\Delta\mu_{ge}$ values of $\mathbf{II}[0]$ and $\mathbf{I}[0]$ are inverted. Strikingly, the \mathbf{II}' series displays very weak dipole moment variations compared to the other series. As indicated by the d^{CT} values collected in Table 6, these weak $\Delta\mu_{ge}$ values result from small charge transfer distances, the latter being the consequence of a larger spatial overlap between the HOMO and LUMO, and thus to more localized changes in the electron density upon the $S_0 \rightarrow S_1$ transition (see the density difference maps in the supporting information). The smaller $\Delta\mu_{ge}$ values obtained for the \mathbf{II}' series also confirm that these chromophores are closer to the cyanine limit. As mentioned in the introduction, the cyanine limit refers to push-pull dyes for which the ground-state wavefunction has equal weight of the DA and D^+A^- resonance forms. Within the two-state approximation, the ground and excited state dipole moments are respectively expressed as $\mu_g = \delta\mu_Z$ and $\mu_e = (1 - \delta)\mu_Z$, where δ is the formal ground state charge transfer between the D and A units (see Eq. 1), and μ_Z is the dipole moment of the D^+A^- resonance form. In the cyanine limit, the amount of intramolecular CT between the D and A units in the ground state is formally equal to 0.5, so that $\Delta\mu_{ge} = 0$. The formal ground-state charge transfer values between D and A, evaluated from the ratio between the ground and excited state dipole moments as $\delta = \mu_g / (\mu_g + \mu_e)$, are reported in the last column of Table 6. The δ values, close to 0.5 and constant when increasing the chain length, further illustrate the better

conjugation in chromophores belonging to the **II'** series. All other compounds display smaller δ values, which progressively decrease with n in series **I** and **I'**.

VI. Nonlinear optical properties

The evolution with respect to the length of the polyenic chain of the total HRS hyperpolarizabilities (β_{HRS}), as well as of the main diagonal component of the β tensor (evaluated as $\beta_{zzz} \approx \sqrt{35/6} \beta_{HRS}$), is reported in Figure 5 for the four series of chromophores. The numerical values of β_{HRS} and β_{zzz} are given in Table 7, together with the results obtained from TDDFT calculations. All β values are given according to the convention of Ref. 19. The experimental HRS data evidence a strong enhancement of β_{HRS} and β_{zzz} with increasing chain length, which is particularly pronounced for chromophores bearing the strong acceptor group A2 implying a phthalimide substituent. The nature of the donor group has a smaller impact on the NLO enhancement, although, for the same polyenic chain length, the β_{HRS} responses of chromophores having the stronger donor D2 (series **I'** and **II'**) are larger than those involving D1 (series **I** and **II**). This results in the remarkable enhancement within the **II'** series (see $\beta_{HRS}[n]/\beta_{HRS}[0]$ ratios in Table 7), and to the record β_{HRS} response of **II'**[4]. As already noticed in our previous paper,⁷ this huge HRS response is striking for a cyanine-like derivative, which is expected to show a very low quadratic NLO response due to vanishing $\Delta\mu$ and BLA values. This apparent breaking of the 2-state model should however be nuanced because the magnitude of the NLO response partly originates from resonance effects, the second-harmonic wavelength (954 nm for laser pulses at 1907 nm) lying within the main absorption band of the largest compounds ($\lambda_{max} = 916$ nm for **II'**[3], see Table 6 and Figure 3). To estimate the intrinsic β responses of the dyes, the HRS hyperpolarizabilities

measured at 1907 nm were extrapolated to the static limit (*i.e.* at infinite wavelength), by using a homogeneously damped frequency dispersion factor expressed as:²⁰

$$F(\omega) = \frac{\Delta E_{ge}^2 (\Delta E_{ge} - i\Gamma)^2}{\left[(\Delta E_{ge} - i\Gamma)^2 - (\hbar\omega)^2 \right] \left[(\Delta E_{ge} - i\Gamma)^2 - (2\hbar\omega)^2 \right]} \quad (4)$$

where $\hbar\omega$ is the photon energy of the incident beam, and Γ a homogeneous broadening parameter. To account for the change in the absorption bandwidth from one compound to another, the value of the damping factor Γ was set equal to 1.2 times the half width at half maximum of the first absorption band (HWHM = FWHM/2, see Table 6), in line with previous studies.²¹ The static HRS responses, estimated as $\beta_{HRS,0} = \beta_{HRS}/F(\omega)$ (Table 7) are smaller than the dynamic ones ($F(\omega) > 1$), and also show significant enhancement when increasing the chain length. However, the frequency dispersion factors estimated in the **II'** series are larger than in the other series (increasing with chain length from 1.5 to 3.0), so that removing frequency dispersion effects in this series induces a larger decrease of the β response than in the others. As a result, for a same chain length ($n = 2$), the static $\beta_{HRS,0}$ values involve in the order **I** \approx **I'** < **II'** < **II**, differing from that of the dynamic ones (**I** < **I'** < **II** < **II'**).

The progressive increase with chain length of the dynamic HRS hyperpolarizabilities is qualitatively reproduced by the TDDFT calculations. However, the calculated enhancement factors $\beta_{HRS}[n]/\beta_{HRS}[0]$ (Table 7) are overestimated compared to experiments in series **I** and **I'**, due to the systematic overestimation of the transition energies by the CAM-B3LYP XCF (see Table 6). In series **II** and **II'**, the TD-DFT calculations instead underestimate the enhancement factors beyond $n = 2$, leading to the **II'** < **I'** < **I** < **II** hierarchy for the computed dynamic β_{HRS} values of polye[n]enic compounds with $n = 2$. This hierarchy is preserved when considering the static β_{HRS} values ($\beta_{HRS,0}^{calc}$, see Table 6) and differs from that obtained

from HRS measurements, which demonstrates that the discrepancies between experiments and theory cannot be only ascribed to frequency resonance effects. Note that, although underestimated, the static HRS responses estimated using the 2-state approximation ($\beta_{HRS}^{TSA} = \sqrt{6^3/35} \beta_{zzz}^{TSA}$, with β_{zzz}^{TSA} evaluated using the quantities gathered in Table 6 following Eq. 2), leads to a similar hierarchy to that found from full TDDFT calculations, demonstrating that the 2-state approximation provides reasonable trends within the investigated series. Finally, TDDFT calculations also evidence that increasing the conjugation length reinforces the 1D character of the NLO response, as indicated by the progressive increase of the $\beta_{zzz}^{calc} / \beta_{zzz}^{1D}$ ratios (see Table 6).

VII. Conclusions

New dipolar tricyanopropylidene-based merocyanine dyes containing different pairs of push/pull units linked through polyenic bridges of different lengths have been synthesized. Within each series, the evolution of the structural as well as of the linear and nonlinear optical properties with respect to the polyenic chain length have been characterized by combining complementary spectroscopy techniques and first principle calculations. ^1H NMR measurements revealed that chromophores incorporating a phthalimide substituent within the tricyanopropylidene withdrawing moiety (**II** and **II'**) display smaller bond length alternation along the conjugated linker than those including a smaller amine function (**I** and **I'**). Moreover, using a dihexylaminothiophenyl fragment (**I'** and **II'**) as a push moiety further reduces the BLA compared to substitution using a dihexylaminophenyl fragment (**I** and **II**). As a consequence, the largest compounds of the **II'** series incorporating the most efficient donor/acceptor pair exhibit a cyanine-like electronic structure, with negligible BLA. The alteration of the BLA with the nature of the donor/acceptor units induces marked shifts in the intramolecular charge transfer absorption bands. Within a series, successive vinylogations

also induce significant redshifts of the absorption maximum, associated with large increases of the second-harmonic responses. Despite displaying negligible BLA, compounds of the **II'** series exhibit the highest second-order hyperpolarizabilities for a given chain length, which apparently breaks the paradigm of optimal BLA predicted by the 2-state approximation. DFT calculations qualitatively reproduce the evolution of the linear and nonlinear optical properties with chain length, and provide fundamental insights onto the relationship between the chemical structure of the dyes and their optical properties. In particular, the computed geometrical structures and dipole moment variations confirm the cyanine-like structure of the **II'** series. However, DFT calculations do not reproduce the experimental measurements regarding the relative ordering of the hyperpolarizabilities of the different series, and more specifically the particularly marked enhancement of the NLO response of **II'**, which partly originate from frequency dispersion effects. Finally, DSC measurements show that all derivatives display reasonable thermal stabilities. Therefore, owing to their large NLO responses, reasonable thermal stabilities and full transparency at telecommunication wavelengths, these dipolar dyes appear highly promising for various NLO applications.

Supporting Information

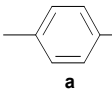
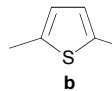
Synthesis and characterization of merocyanines dyes of series **I** and **II**. HOMO and LUMO shapes and density difference maps. Hyper-Rayleigh scattering experimental details.

Acknowledgements

MBD and PKD thank the Indo-French Centre for Promotion of Advanced Research (IFCPAR)/Centre Franco-Indien pour la Promotion de la Recherche Avancée (CEFIPRA) (Project: 3505-1, Supramolecular Interactions in Multichromophores) for financial support,

and a PDF to VP. MBD gratefully acknowledges financial support from Conseil Régional d'Aquitaine (Chaire d'accueil grant). The calculations were performed on the “Mésocentre de Calcul Intensif Aquitain” (MCIA) of the University of Bordeaux, financed by the Conseil Régional d'Aquitaine and the French Ministry of Research and Technology.

Table 1. Summary of the results of vinylogation and condensation reactions.

	n	Aldehyde	Yield ^a (%)	Chromophore	Yield ^b (%)	Chromophore	Yield ^c (%)
 a	0	3a[0]	-	I[0]	62	II[0]	80
	1	3a[1]	76 68 ^d	I[1]	85	II[1]	83
	2	3a[2]	55 74 ^d	I[2]	69	II[2]	66
 b	0	3b[0]	-	I'[0]	65	II'[0]	70
	1	3b[1]	97	I'[1]	74	II'[1]	65
	2	3b[2]	88	I'[2]	58	II'[2]	72 ^e
	3	3b[3]	83	I'[3]	71	II'[3]	50 ^e
	4	3b[4]	76	I'[4]	65		

^a Isolated yield of the vinylogation step (method A): **3[n-1]** → **3[n]**. ^b Isolated yield in chromophore **I** and **I'**. ^c Isolated yield in case of chromophore **II** and **II'**. ^d Isolated yields by method B. ^e Accompanied by a cyclization side-product⁹.

Table 2. ^1H - ^1H coupling constants ($^3J_{\text{HH}}$, Hz) between vicinal protons along the polyenic chain of the push-pull poly[n]enes,^a and average difference in the $^3J_{\text{HH}}$ values of adjacent C=C and C-C bonds (ΔJ_{av} , Hz).

Compd	J_{12}	J_{23}	J_{34}	J_{45}	J_{56}	J_{67}	J_{78}	J_{89}	ΔJ_{av}
I[0]									-
I[1]	14.7	11.7							3.0
I[2]	15.1	10.9	14.0	11.8					3.2
I'[0]									-
I'[1]	13.5	12.3							1.4
I'[2]	14.0	11.9	13.3	12.1					1.6
I'[3]	14.4	11.5	13.9	12.1	13.4	11.8			2.1
I'[4]	14.4	11.7	14.5	11.4	13.9	12.0	13.7	11.9	2.4
II[0]									-
II[1]	14.3	12.2							2.1
II[2]	14.7	11.9	13.1	13.1					1.4
II'[0]									-
II'[1]	13.0	13.0							0.0
II'[2]	12.8	12.5	13.0	13.0					0.2
II'[3]	13.6	13.6	13.0	13.0	13.8	13.8			0.0

^a the atom numbering starts from the donor end to the acceptor end along the polyenic chain.

Table 3. Variation of ΔJ_{av} (Hz) with solvents of varying polarity for **I**, **I'**, **II**, **II'**[1].

Solvent	I [1]	I' [1]	II [1]	II' [1]
C ₆ D ₆	3.4	2.1	2.6	0.0
CDCl ₃	3.0	1.4	2.1	0.0
C ₃ D ₆ O	3.3	1.9	2.0	0.0

Table 4. Bond Length Alternation along the conjugated carbon chain (Å), HOMO and LUMO energies and gaps (eV), and ground state dipole moments (D), as calculated at the B3LYP/6-311G(d) level in chloroform for the merocyanine dyes **I**, **I'**[n] and **II**, **II'**[n].

	BLA	E_{HOMO}	E_{LUMO}	E_{GAP}	μ_g
I [0]	0.071	-5.850	-2.667	3.184	13.49
I [1]	0.053	-5.605	-2.884	2.721	16.29
I [2]	0.048	-5.442	-3.020	2.422	18.89
I' [0]	0.045	-5.714	-2.667	3.048	14.86
I' [1]	0.032	-5.442	-2.857	2.585	18.73
I' [2]	0.030	-5.279	-2.993	2.286	22.11
I' [3]	0.030	-5.143	-3.102	2.041	25.19
I' [4]	0.031	-5.022	-3.162	1.860	27.98
II [0]	0.055	-5.905	-3.184	2.721	13.24
II [1]	0.035	-5.687	-3.320	2.367	17.00
II [2]	0.030	-5.524	-3.401	2.122	20.68
II' [0]	0.023	-5.823	-3.129	2.694	15.29
II' [1]	0.010	-5.578	-3.238	2.340	20.64
II' [2]	0.008	-5.388	-3.347	2.041	25.49
II' [3]	0.008	-5.252	-3.401	1.850	30.24

Table 5. Thermal stability data for the push-pull polyenes **I**, **I'**, **II** and **II'** from DSC experiments.^a

Compd	T_g	T_c	T_m	T_{od}	T_d
I [0]	/	/	194	258	275
I [1]	/	138	158	203	>220
I [2]	101	/	176	206	235
I' [0]	/	/	103	242	275
I' [1]	/	/	146	195	>200
I' [2]	138	/	191	196	207
I' [3]	101	/	131	147	166
I' [4]	/	/	145	149	158
II [0]	120	/	171	185	196
II [1]	100	/	185	191	200
II [2]	104	/	148	152	>160
II' [0]	110	/	154	250	269
II' [1]	115	132	160	234	254
II' [2]	98	140	205	207	>215
II' [3]	128	/	192	204	210

^a T_g -glass transition temperature; T_c -crystallization temperature; T_m -melting temperature; T_{od} -onset of decomposition and T_d -decomposition exotherm. The experiment was run under nitrogen gas atmosphere at a heating rate of 10 °C per minute.

Table 6. Linear optical properties of chromophores **I**, **I'**, **II**, **II'**. Maximal absorption wavelength (λ_{\max} , nm), oscillator strength^a (f_{\max}), molar extinction coefficient ($\log \epsilon_{\max}$), and full width at half maximum (FWHM, cm^{-1}) measured in CHCl_3 . Maximal absorption wavelength (λ_{ge} , nm), oscillator strength (f_{ge}), weight of the HOMO to LUMO excitation (%H \rightarrow L), transferred charge (q^{CT} , |e|), charge transfer distance (d^{CT} , Å), dipole moment variation ($\Delta\mu_{\text{ge}}$, D), and formal ground-state charge transfer^b (δ , |e|), calculated at the TDDFT/CAM-B3LYP/6-311+G(d) level.

Cpd	λ_{\max}	$\log \epsilon_{\max}$	FWHM	f_{\max}	λ_{ge}	μ_{ge}	f_{ge}	%H \rightarrow L	q^{CT}	d^{CT}	$\Delta\mu_{\text{ge}}$	δ^c
I [0]	470	4.62	3400	0.61	410	10.31	1.22	95	0.53	2.28	5.80	0.41
I [1]	529	4.68	4700	0.97	478	13.12	1.69	94	0.56	2.92	7.81	0.40
I [2]	565	4.62	5100	0.91	537	15.70	2.16	92	0.59	3.61	10.18	0.39
I' [0]	515	4.87	1900	0.61	448	10.21	1.09	97	0.44	1.05	2.23	0.47
I' [1]	614	5.00	1700	0.73	527	13.47	1.62	96	0.46	1.49	3.32	0.46
I' [2]	704	4.79	3000	0.80	599	16.48	2.13	95	0.50	2.36	5.68	0.44
I' [3]	712	4.70	4500	0.97	663	19.23	2.62	94	0.55	3.30	8.67	0.42
I' [4]	720	4.57	5100	0.81	720	21.72	3.08	93	0.60	4.28	12.27	0.40
II [0]	566	4.88	2200	0.72	474	11.31	1.27	89	0.57	2.57	6.99	0.39
II [1]	668	5.03	2050	0.94	553	14.41	1.77	93	0.56	2.79	7.48	0.41
II [2]	759	4.87	2800	0.89	622	17.25	2.25	93	0.58	3.20	8.85	0.41
II' [0]	581	5.05	1300	0.63	508	11.34	1.19	97	0.45	0.86	1.84	0.47
II' [1]	690	5.23	900	0.66	593	14.76	1.73	96	0.45	0.62	1.33	0.48
II' [2]	803	5.43	830	0.96	675	17.99	2.25	95	0.47	0.79	1.78	0.48
II' [3]	916	5.24	800	0.60	756	21.11	2.77	94	0.49	1.14	2.67	0.48

^a evaluated as $f_{\max} \approx 4.3 \times 10^{-9} \times \epsilon \times \text{FWHM}$. ^b evaluated as $\delta = \mu_g / (\mu_g + \mu_e)$.

Table 7. Nonlinear optical properties of the push-pull chromophores in CHCl₃. All β values are given in 10⁻³⁰ esu. The ratios $R = \beta_{HRS}[n]/\beta_{HRS}[0]$ measure the relative enhancement of β_{HRS} with chain length.

Compd	$\beta_{HRS}^{exp a}$	R^{exp}	$\beta_{HRS,0}^{exp b}$	$\beta_{zzz}^{exp c}$	$\beta_{HRS}^{calc d}$	R^{calc}	$\beta_{HRS,0}^{calc d}$	$\beta_{zzz}^{calc d}$	$\beta_{HRS}^{TSA e}$	$\beta_{zzz}^{1D f}$	%1D ^g
I[0]	12	/	10	29	61	/	64	125	65	147	85
I[1]	19	1.6	16	46	168	2.8	165	367	193	405	91
I[2]	37	3.1	30	89	388	6.4	352	888	455	937	95
I'[0]	18	/	14	43	41	/	45	88	29	100	88
I'[1]	22	1.2	15	53	119	2.9	122	265	105	288	92
I'[2]	51	2.8	32	123	342	8.3	314	788	348	826	95
I'[3]	148	8.2	107	357	881	21.5	711	2076	886	2129	97
I'[4]	865	48.1	714	2090	2029	49.5	1404	4904	1886	4902	100
II[0]	44	/	32	106	110	/	110	207	126	266	78
II[1]	56	1.3	36	135	283	2.6	259	587	299	685	86
II[2]	574	13.0	344	1386	648	5.9	529	1425	640	1565	91
II'[0]	47	/	32	114	52	/	56	92	38	127	72
II'[1]	78	1.7	44	188	102	2.0	105	176	64	246	72
II'[2]	630	13.4	282	1522	235	4.5	213	441	165	568	78
II'[3]	3900	83.0	1280	9420	611	11.8	456	1272	427	1476	86

^a derived from HRS measurements at 1.907 μm in chloroform. ^b extrapolated using the 2-state damped model. ^c evaluated as $\beta_{zzz}^{exp} \approx \sqrt{35/6} \beta_{HRS}^{exp}$. ^d calculated at the CAM-B3LYP/6-311+G(d) level in chloroform. ^e evaluated using $\beta_{HRS}^{TSA} = \sqrt{6^3/35} \beta_{zzz}^{TSA}$. ^f evaluated as $\beta_{zzz}^{1D} \approx \sqrt{35/6} \beta_{HRS}^{calc}$. ^g evaluated as $\beta_{zzz}^{calc} / \beta_{zzz}^{1D} \times 100$.

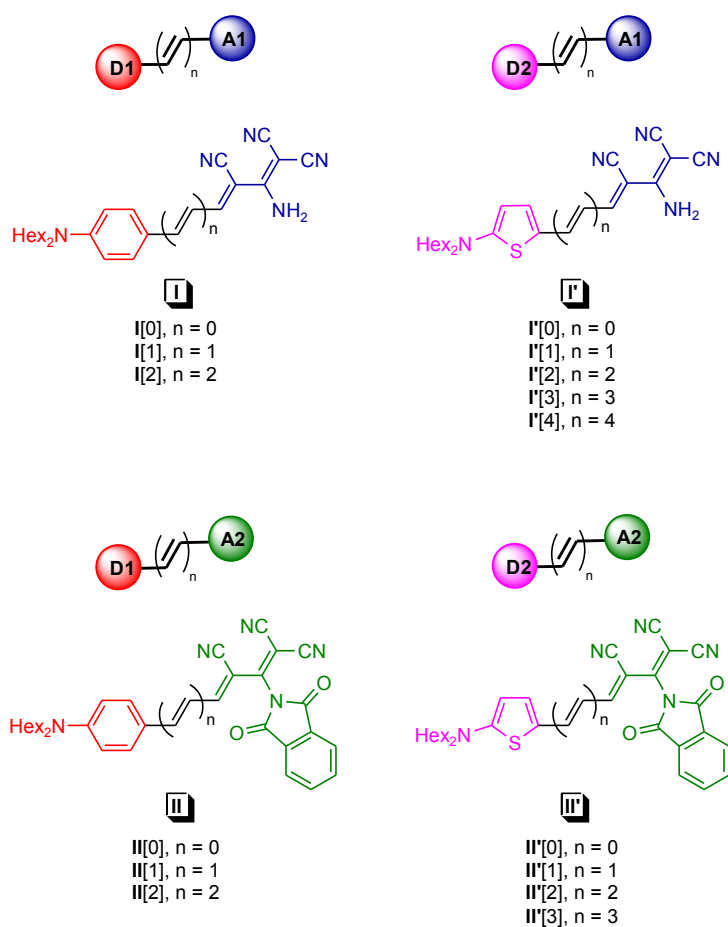
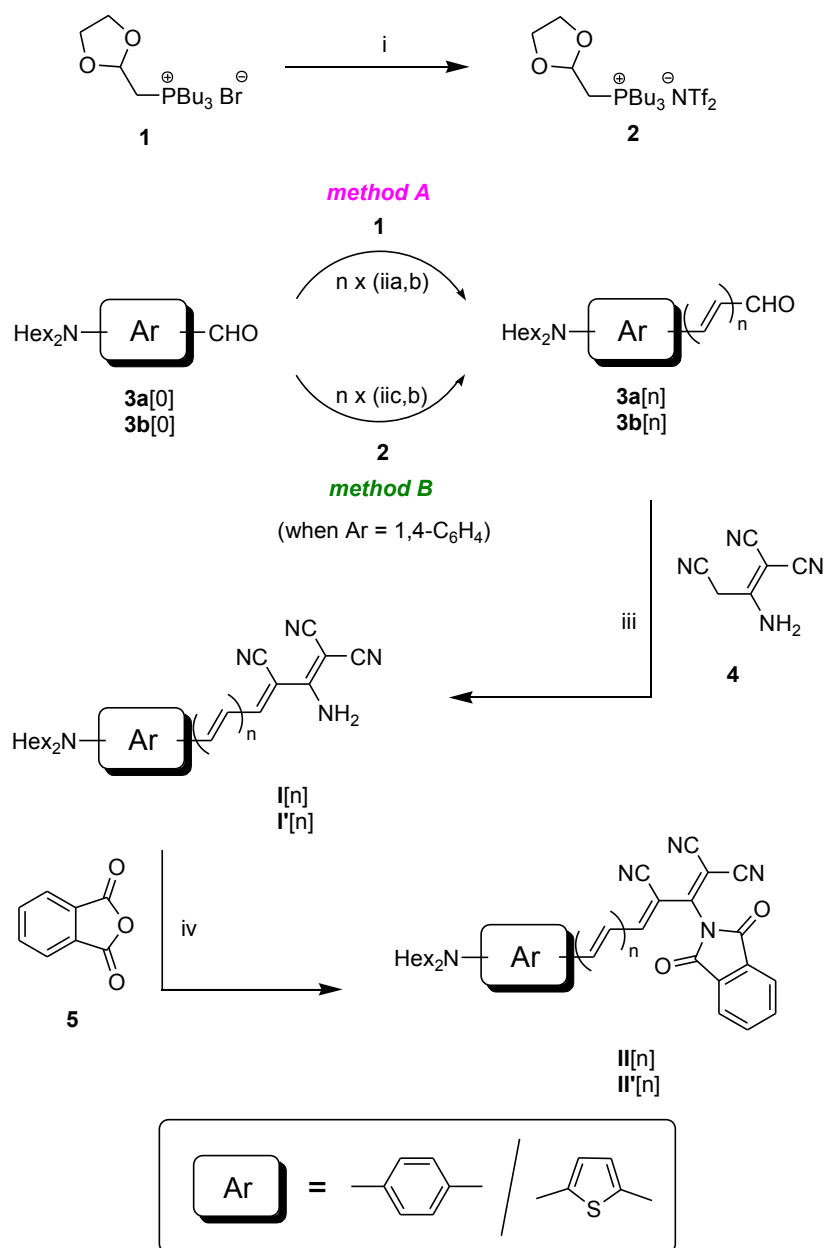


Chart 1. Structures of the merocyanine derivatives investigated in this study.



Reagents and conditions: (i) LiNTf₂, H₂O, rt, 8 h; (ii)a) **1** (1.1 equiv), NaH, THF, rt, overnight; b) HCl, THF, rt; c) **2** (1.1 equiv), NaH, 100 °C, 1-2 h; (iii) **4** (1.0 equiv), EtOH, reflux, 2-4 h; (iv) **5** (3.0 equiv), Et₃N (3.0 equiv), CH₂Cl₂, 50-60 °C, 3-6 h.

Scheme 1. Synthesis of series of merocyanine derivatives **I**, **I'**, **II** and **II'**.

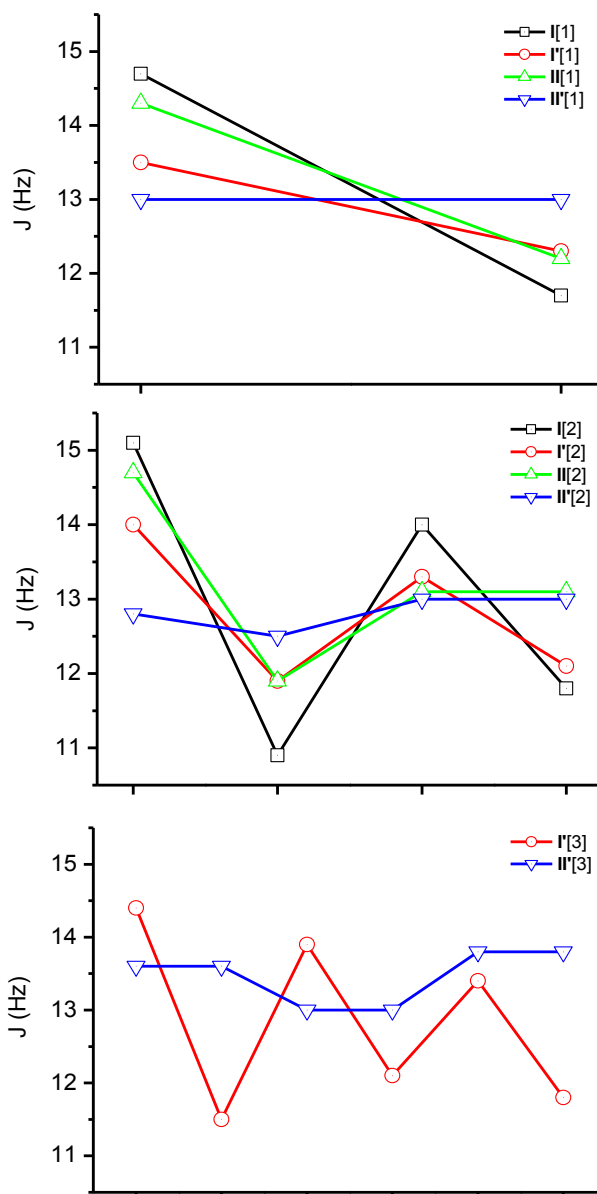


Figure 1. Oscillatory behavior of the coupling constants of the push-pull poly[n]enes with $n = 1$ (top), $n = 2$ (middle), and $n = 3$ (bottom).

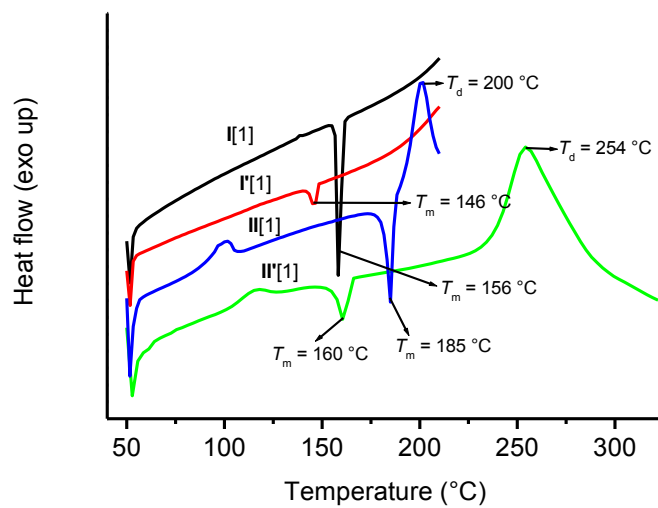


Figure 2. DSC scans of the push-pull poly[n]enes **I**, **I'**, **II** and **II'** with $n = 1$.

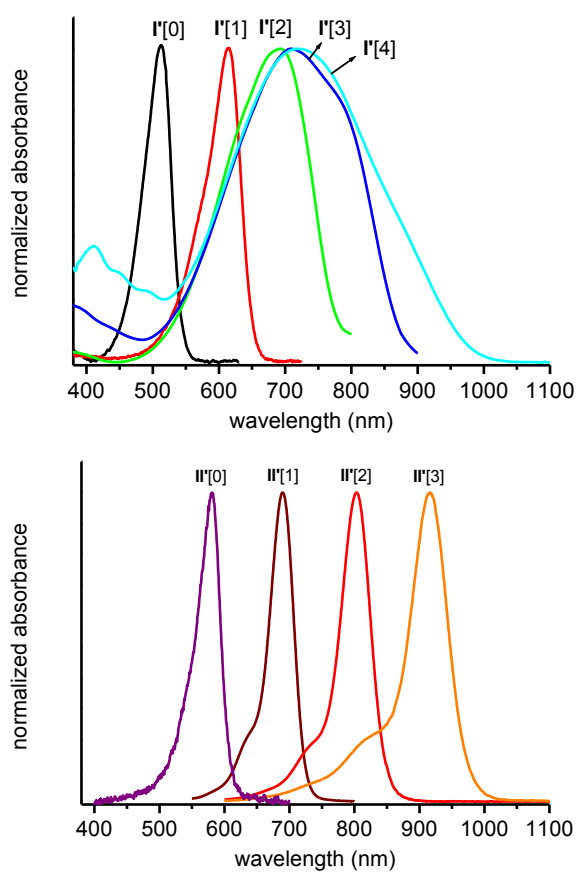


Figure 3. UV-vis absorption spectra of the push-pull poly[n]enes **I'** (top) and **II'** (bottom) in chloroform.

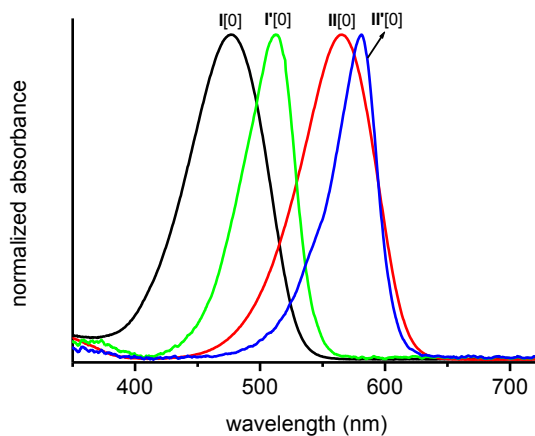


Figure 4. UV-vis absorption spectra of push-pull poly[n]enes ($n = 0$) **I**, **I'**, **II**, and **II'** in chloroform.

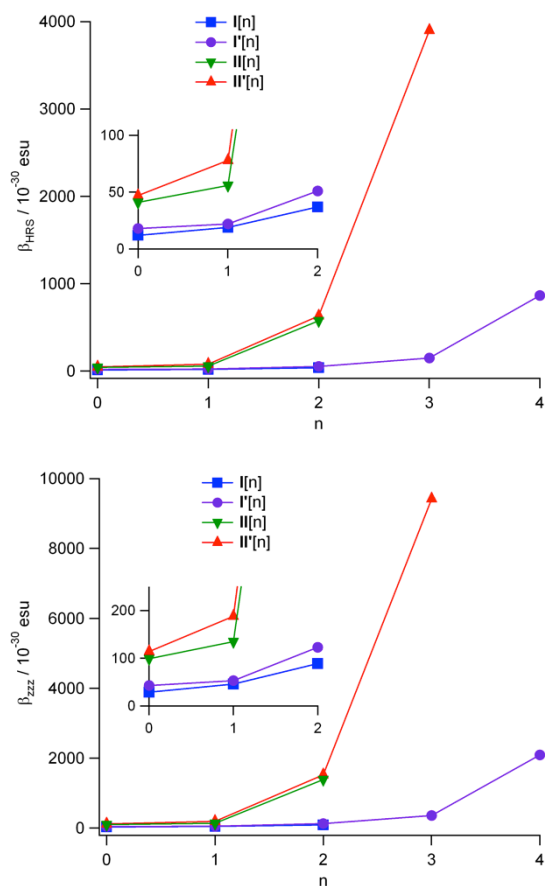


Figure 5. Variation of β_{HRS} (top) and β_{zzz} (bottom) in CHCl_3 with the polyenic chain length n . Insets show zoomed portions of the plots for small n values.

References

- [1] L. R. Dalton, P. A. Sullivan, D. H. Bale, *Chem. Rev.*, **2010**, *110*, 25-55 and references cited therein.
- [2] a) P. J. Campagnola, M-d. Wei, A. Lewis, L. M. Loewe, *Biophys. J.*, **1999**, *77*, 3341-3349; b) L. Moreaux, O. Sandre, S. Charpak, M. Blanchard-Desce, J. Mertz, *Biophys. J.*, **2001**, *80*, 1568-157; c) D. A. Dombeck, M. Blanchard-Desce, W. W. Webb, *J. Neuroscience*, **2004**, *24*, 999-1003; d) J. E. Reeve, H. L. Anderson, K. Clays, *Phys. Chem. Chem. Phys.*, **2010**, *12*, 13484–13498.
- [3] a) D. A. Parthenopoulos, P. M. Renzepis, *Science* **1989**, *245*, 843-845; b) C. C. Corredor, Z.-L. Huang, K. D. Belfield, A. R. Morales, M. V. Bondar, *Chem. Mater.* **2007**, *19*, 5165-5173; c) Themed issue on organic nonlinear optics, S. R. Marder, Guest Ed., *J. Mater. Chem.* **2009**, *19*, 7381-7568.
- [4] a) M. Blanchard-Desce, *C. R. Phys.* **2002**, *3*, 439-448; b) D. R. Larson, W. R. Zipfel, R. M. Williams, S. W. Clark, M. P. Bruchez, F. W. Wise, W. W. Webb, *Science* **2003**, *300*, 1434-1437; c) R. K. Tathavarty, M. Parent, M. H. V. Werts, S. Gmouh, A.-M. Caminade, L. Moreaux, S. Charpak, J.-P. Majoral, M. Blanchard-Desce, *Angew. Chem. Int. Ed.*, **2006**, *45*, 4645-4648; d) H. M. Kim, B. R. Cho, *Acc. Chem. Res.* **2009**, *42*, 863-872; e) E. De Meulenaere, I. Asselberghs, M. de Wergifosse, E. Botek, S. Spaepen, B. Champagne, J. Vanderleyden and K. Clays *J. Mater. Chem.*, **2009**, *19*, 7514-7519; f) J.E. Reeve, H.L. Anderson, K. Clays, *Phys. Chem. Chem. Phys.* **2010**, *12*, 13484-13498; g) V. Parthasarathy, S. Fery-Forgues, E. Campioli, G. Recher, F. Terenziani, M. Blanchard-Desce, *Small*, **2011**, *7*, 3219–3229; h) S. Yao, K. D. Belfield, *Eur. J. Org. Chem.* **2012**, *2012*, 3199-3217; i) C. Le Droumaguet, A. Sourdon, E. Genin, O. Mongin, M. Blanchard-Desce, *Chem. Asian J.*, **2013**, *8*, 2984-3001.

- [5] a) J. L. Brédas, F. Meyers, B. M. Pierce, J. Zyss *J. Am. Chem. Soc.* **1992**, *114*, 4928-4929; b) I. Asselberghs, G. Hennrich, K. Clays *J. Phys. Chem. A* **2006**, *110*, 6271-6275; c) H. M. Kim, B. R. Cho *J. Mater. Chem.*, **2009**, *19*, 7402-7409; d) Y. M. Poronik, V. Hugues, M. Blanchard-Desce, D. T. Gryko, *Chem. Eur. J* **2012**, *18*, 9258; e) F. Castet, M. Blanchard-Desce, F. Adamietz, Y. M. Poronik, D. T. Gryko, V. Rodriguez *Chem. Phys. Chem.* **2014**, *15*, 2575–2581.
- [6] a) D. R. Kanis, M. A. Ratner, T. S. Marks, *Chem. Rev.* **1994**, *94*, 195; b) J. L. Brédas, C. Adant, P. Tackx, A. Persoons, B. M. Pierce *Chem. Rev.* **1994**, *94*, 243; c) S. R. Marder, L. T. Cheng, B. G. Tiemann, A. C. Friedli, M. Blanchard-Desce, J. W. Perry, J. Skindhøj, *Science* **1994**, *263*, 511-514; d) S. Beckmann, K.-H. Etzbach, P. Krämer, K. Lukaszuk, R. Matschiner, A. J. Schmidt, P. Schuhmacher, R. Sens, G. Seybold, R. Wortmann, F. Würthner, *Adv. Mater.* **1999**, *11*, 536–541; e) A. Plaquet, B. Champagne, J. Kulhanek, F. Bures, E. Bogdan, F. Castet, L. Ducasse, V. Rodriguez, *Chem. Phys. Chem.* **2011**, *12*, 3245.
- [7] V. Parthasarathy, R. Pandey, M. Stolte, S. Ghosh, F. Castet, F. Würthner, P. K. Das, M. Blanchard-Desce, *Chem. Eur. J.* **2015**, *21*, 14211–14217.
- [8] a) J. A. Davies, A. Elangovan, P. A. Sullivan, B. C. Olbricht, D. H. Bale, T. R. Ewy, C. M. Isborn, B. E. Eichinger, B. H. Robinson, P. J. Reid, X. Li, L. R. Dalton, *J. Am. Chem. Soc.* **2008**, *130*, 10565-10575; b) S.-H. Jang, J. Luo, N. M. Tucker, A. Leclercq, E. Zojer, M. A. Haller, T.-D. Kim, J.-W. Kang, K. Firestone, D. Bale, D. Lao, J. B. Benedict, D. Cohen, W. Kaminsky, B. Kahr, J.-L. Brédas, P. Reid, L. R. Dalton, A. K.-Y. Jen, *Chem. Mater.* **2006**, *18*, 2982-2988.
- [9] V. Parthasarathy F. Castet, R. Pandey, O. Mongin, P. K. Das, M. Blanchard-Desce, *Dyes and Pigments*, **2016**, *130*, 70-78.
- [10] a) D. Jacquemin, A. Femenias, H. Chermette, I. Ciofini, C. Adamo, J. M. André, E. R. Perpète, *J. Phys. Chem. A* **2006**, *110*, 5952; b) J. C. Sancho-García, A. J. Pérez-Jiménez,

- Phys. Chem. Chem. Phys.* **2007**, *9*, 5874; c) D. Jacquemin, C. Adamo, *J. Chem. Theory Comput.* **2011**, *7*, 369-376; d) T. Körzdörfer, R. M. Parrish, J. S. Sears, C. D. Sherrill, J. L. Brédas, *J. Chem. Phys.* **2012**, *137*, 124305; e) E. F. Oliveira, J. C. Roldao, B. Milián-Medina, F. C. Lavarda, J. Gierschner, *Chem. Phys. Lett.* **2016**, *645*, 169-173.
- [11] T. Yanai, D. Tew, N. Handy *Chem. Phys. Lett.* **2004**, *393*, 51-57.
- [12] a) D. Jacquemin, V. Wathelet, E. A. Perpète, C. Adamo, *J. Chem. Theory Comput.* **2009**, *5*, 2420; b) A. D. Laurent, D. Jacquemin *Int. J. Quant. Chem.* **2013**, *113*, 2019-2039.
- [13] a) L. E. Johnson, L. R. Dalton, B. H. Robinson, *Acc. Chem. Res.* **2014**, *47*, 3258-3265; b) F. Castet, B. Champagne, F. Pina, V. Rodriguez *Chem. Phys. Chem.* **2014**, *15*, 2221.
- [14] J. Tomasi, B. Mennucci, R. Cammi, *Chem. Rev.* **2005**, *105*, 2999-3094.
- [15] Gaussian 09, Revision D.01, M. J. Frisch *et al.* Gaussian, Inc., Wallingford CT, 2009.
- [16] M. Blanchard-Desce, V. Alain, P. V. Bedworth, S. R. Marder, A. Fort, C. Runser, M. Barzoukas, S. Lebus, R. Wortmann, *Chem. Eur. J.* **1997**, *3*, 1091-1104.
- [17] a) J. Luo, X.-H. Zhou, A. K.-Y. Jen, *J. Mater. Chem.* **2009**, *19*, 1201-1205; b) O. Ostroverkhova, D. Wright, U. Gubler, W. E. Moerner, M. He, A. Sastre-Santos, R. J. Twieg, *Adv. Funct. Mater.* **2002**, *12*, 621-629.
- [18] a) T. Le Bahers, C. Adamo, I. Ciofini, *J. Chem. Theory Comput.*, **2011**, *7*, 2498-2506; b) D. Jacquemin, T. Le Bahers, C. Adamo, I. Ciofini, *Phys. Chem. Chem. Phys.*, **2012**, *14*, 5383-5388.
- [19] A. Willetts, J. E. Rice, D. M. Burland, D. P. Shelton, *J. Chem. Phys.* **1992**, *97*, 7590.
- [20] a) J. L. Oudar, D. S. Chemla, *J. Chem. Phys.* **1977**, *66*, 2664-2668 ; b) J. Campo, W. Wenseleers, E. Goovaerts, M. Szablewski, G. H. Cross, *J. Phys. Chem. C* **2008**, *112*, 287-296.
- [21] a) B. F. Levine, C. G. Bethea, E. Wasserman, L. Leenders, *J. Chem. Phys.* **1978**, *68*, 5042; b) P. M. Lundquist, S. Yitzchaik, T. J. Marks, G. K. Wong, S. DiBella, R. Cohen, G. Berkovic, *Phys. Rev. B* **1997**, *55*, 14055; c) G. Berkovic, G. Meshulam, Z. Kotler, *J. Chem.*

Phys. **2000**, *112*, 3997-4003; d) F. Mançois, J.-L. Pozzo, J. Pan, F. Adamietz, V. Rodriguez, L. Ducasse, F. Castet, A. Plaquet, B. Champagne *Chem. Eur. J.*, **2009**, *15*, 2560-2571; e) P. Beaujean, F. Bondu, A. Plaquet, F. Raymo, F. Castet, V. Rodriguez, B. Champagne *J. Am. Chem. Soc.* **2016**, *138*, 5052-5062.